MOLECULAR AND CELLULAR BIOLOGY, June 2007, p. 4121–4132 Vol. 27, No. 11
0270-7306/07/$08.00+0 doi:10.1128/MCB.01708-06

Combinatorial Expression of α- and γ-Protocadherins Alters Their Presenilin-Dependent Processing▽

Stefan Bonn, Peter H. Seeburg,* and Martin K. Schwarz

Department of Molecular Neurobiology, Max Planck Institute for Medical Research, Jahnstrasse 29, 69120 Heidelberg, Germany

Received 11 September 2006/Returned for modification 27 November 2006/Accepted 19 March 2007

α- and γ-protocadherins (Pcdhs) are type I transmembrane receptors expressed predominantly in the central nervous system and located in part in synapses. They are transcribed from complex genomic loci, giving rise in the mouse to 14 α-Pcdh and 22 γ-Pcdh isoforms consisting of variable domains, each encompassing the extracellular region, the transmembrane region, and part of the intracellular region harboring the α- or γ-Pcdh-specific invariant cytoplasmic domain. Presenilin-dependent intramembrane proteolysis (PS-IP) of γ-Pcdhs and the formation of α/γ-Pcdh heteromers led us to investigate the effects of homo- and heteromer formation on γ- and putative α-Pcdh membrane processing and signaling. We find that upon surface delivery, α-Pcdhs, like γ-Pcdhs, are subject to matrix metallo-protease cleavage followed by PS-IP in neurons. We further demonstrate that the combinatorial expression of α- and γ-Pcdhs modulates the extent of their PS-IP, indicating the formation of α/γ-Pcdh heteromers with an altered susceptibility to processing. Cell-specific expression of α/γ-Pcdh isoforms could thus determine cell and synapse adhesive properties as well as intracellular and nuclear signaling by their soluble cytoplasmic cleavage products, α C-terminal fragment 2 (α-CTF-2) and γ-CTF-2.

α-, β-, and γ-protocadherins (Pcdhs) are type I transmembrane proteins belonging to the cadherin superfamily. The gene clusters of α-, β-, and γ-Pcdhs are arranged in tandem on human chromosome 5 (48) and mouse chromosome 18 (39, 49). The murine gene locus encoding the α-Pcdh cluster comprises 14 functional variable exons that are each *cis*-spliced to three constant α-specific exons, and the γ-Pcdh cluster comprises 22 functional variable exons that are *cis*-spliced to three constant γ-specific exons (41, 43). In contrast, the gene locus encoding the β-Pcdh cluster comprises 22 variable exons but lacks constant exons. Thus, each of the 14 possible α-Pcdh and the 22 γ-Pcdh proteins consists of a variable domain encompassing the extracellular region, the transmembrane region, and part of the intracellular region harboring the α- or γ-specific constant intracellular domain. α-Pcdh expression is restricted largely to the central nervous system (CNS) (17), in contrast to the ubiquitous expression of γ-Pcdhs (11). In the CNS, α- and γ-Pcdhs are localized to synapses and are found in postsynaptic density fractions (24). Furthermore, individual neurons can express specific subsets of α- and γ-Pcdhs that form homo- and heteromers in vivo, further increasing the combinatorial power of putative Pcdh complexes in the synapse (3, 16, 17, 24, 41, 43). Since the expression of γ-Pcdhs regulates α-Pcdh surface delivery in heterologous cells (24), α/γ-Pcdh heteromer formation may regulate the abundance of α-Pcdhs at synapses.

The sum of these features, namely, (i) the arrangement of the gene clusters, (ii) cluster diversity, and (iii) the evidence that α- and γ-Pcdhs form heteromers and localize to synapses (17, 24, 29), has rendered Pcdhs attractive candidates for synaptic recognition molecules that could aid in determining the precise patterns of neuronal connectivity (10, 35, 36, 50). Although considerable effort has been directed at unraveling the role of Pcdhs in the formation of specific synaptic contacts, experimental evidence for such a role is still scarce (15).

Regarding γ-Pcdhs, mice without a γ-Pcdh locus die shortly after birth, presumably due to loss of spinal cord interneurons (44). The neonatal death of the γ-*Pcdh*$^{-/-}$ mice precludes the study of mature synaptic contact formation. Furthermore, γ-Pcdhs are subject to matrix metallo-protease (MMP) shedding and presenilin-dependent intramembrane proteolysis (PS-IP), consisting of MMP-mediated shedding of the ectodomain and release of a soluble cytoplasmic domain (γ C-terminal fragment 2 [γ-CTF-2]) by the γ-secretase complex (9, 11) (Fig. 1A). γ-CTF-2 or a further processed part of it seems to locate to the nucleus (9, 11), where it may adopt a signaling function, in analogy to the cytoplasmic domains of prominent targets of γ-secretase, including Notch, APP, N-cadherin, ErbB-4 and SREBP-1 (1, 11, 21, 27, 34, 46). The MMP responsible for constitutive as well as AMPA receptor-regulated ectodomain shedding was found to be *a d*isintegrin *a*nd *m*etallo-protease *10* (ADAM10), which is also responsible for cleavage of Notch, APP, and N- and E-cadherins (12, 18, 22, 30, 31).

Here, we investigated the role of α/γ-Pcdh homo- and heteromer formation on γ-Pcdh and putative α-Pcdh PS-IP in both heterologous cells and neurons. We provide evidence for γ-Pcdh-like cleavage of α-Pcdhs at the cell surface of neurons by consecutive MMP- and γ-secretase-mediated cleavage events. This process releases an intracellular fragment, α-CTF-2, that can also locate to the nucleus, perhaps by its nuclear localization sequence. An MMP responsible for the ectodomain shedding of α-Pcdhs is ADAM10. We find that, in contrast to the situation in heterologous cells, neuronal α-Pcdh

* Corresponding author. Mailing address: Dept. of Molecular Neurobiology, Max Planck Institute for Medical Research, Jahnstrasse 29, 69120 Heidelberg, Germany. Phone: 49-6221-486-495. Fax: 49-6221-486-110. E-mail: seeburg@mpimf-heidelberg.mpg.de.

▽ Published ahead of print on 2 April 2007.

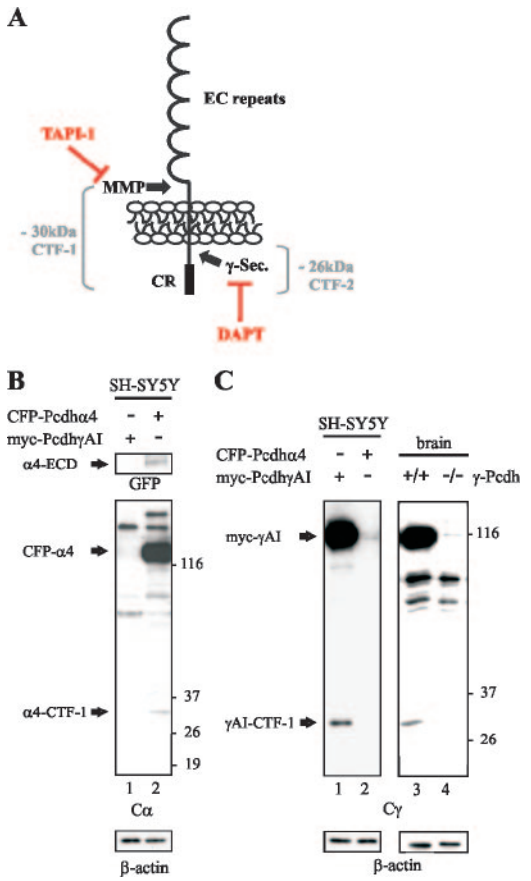

FIG. 1. Expression and processing of Pcdhα4 and PcdhγAI in SH-SY5Y cells. (A) Schematic representation of γ-Pcdh PS-IP. The variable region of α- and γ-Pcdhs consists of six extracellular cadherin repeats (EC repeats), a transmembrane region, and a short intracellular part that is connected to the constant region (CR). The main features of γ-Pcdh PS-IP are an MMP cleavage (blocked by TAPI-1) that generates a soluble ECD and a membrane stump (CTF-1; ~30 kDa) (molecular mass markers [in kilodaltons] are shown on the right), followed by γ-secretase (γ-Sec.) cleavage of the CTF-1 (blocked by DAPT), releasing the intracellular domain (CTF-2; ~26 kDa). (B) Expression scheme for tagged Pcdhs and immunoblots. Middle panel, immunoblot with anti-Cα Ab (Cα) of whole-cell lysates of SH-SY5Y cells transiently expressing myc-PcdhγAI (lane 1) or CFP-Pcdhα4 (lane 2). Arrows indicate the immunoreactive bands detected with Cα Ab for CFP-Pcdhα4 (131 kDa; CFP-α4) and α4-CTF-1 (~30 kDa). Upper panel, immunoblot with anti-GFP Ab (GFP) of corresponding cell culture medium. The arrow indicates the immunoreactive band for the shedded ectodomain of CFP-Pcdhα4 (~100 kDa; α4-ECD). Lower panel, immunoblot of whole-cell lysates with anti-β-actin Ab (β-actin) serving as the loading control. (C) Left upper panel, immunoblot with anti-Cγ Ab (Cγ) of whole-cell lysates of SH-SY5Y cells transiently expressing myc-PcdhγAI (lane 1) or CFP-Pcdhα4 (lane 2). Arrows indicate the immunoreactive bands for myc-PcdhγAI (131 kDa; myc-γAI) and γAI-CTF-1 (~30 kDa). Left lower panel, immunoblot of whole-cell lysates with anti-β-actin Ab (β-actin) serving as the loading control. Above the immunoblots is the scheme for the expression of tagged Pcdhs in SH-SY5Y cells. Right upper panel, immunoblot with anti-Cγ Ab (Cγ) of murine *Pcdhγ*$^{+/+}$ (lane 3) or *Pcdhγ*$^{-/-}$ (lane 4) whole-brain extracts. Right lower panel, immunoblot of corresponding lysates with anti-β-actin Ab (β-actin) serving as the loading control. A scheme representing the genotypes of the mice used for whole-brain protein lysates is shown above the immunoblots.

TABLE 1. α- and γ-Pcdh fusion proteins used in this study[a]

Protein	Characteristics
CFP-Pcdhα4	CFP, 1 2 3 4 5 6, EC domains, TM, α-const.
myc-Pcdhα4	myc, 1 2 3 4 5 6
myc-α-CD	myc
YFP-PcdhγA1	YFP, 1 2 3 4 5 6, EC domains, TM, γ-const.
myc-PcdhγA1	myc, 1 2 3 4 5 6

[a] EC, extracellular cadherin repeats; TM, transmembrane domain; α- or γ-const., α- or γ-Pcdh constant intracellular region, respectively.

surface expression is largely unaffected by the amount of γ-Pcdh expression, as evidenced by regular surface delivery of α-Pcdhs in γ-*Pcdh*$^{-/-}$ neurons. This finding excludes the possibility that γ-*Pcdh*$^{-/-}$ mice die due to a compound loss of α- and γ-Pcdh surface expression. Most notably, neuronal Pcdh susceptibility to processing by MMP shedding and PS-IP depends on the expression of α- and γ-Pcdh isoforms, indicating a role for heteromer formation in the putative signaling of α- and γ-CTF-2s.

MATERIALS AND METHODS

Cell culture, transfections, and drug treatments. SH-SY5Y cells and presenilin 1/2 double-knockout (dko) fibroblasts (13, 14) were cultured in Dulbecco's modified Eagle's medium supplemented with 10% fetal calf serum and 50 mg/liter penicillin-streptomycin in 5% CO_2 at 37°C. Transfections were performed with Lipofectamine 2000 (Invitrogen) according to the manufacturer's instructions. For the detection of shedded α-Pcdh ectodomain, the culture medium of SH-SY5Y cells was replaced 24 h after transfection with low-serum medium (Dulbecco's modified Eagle's medium supplemented with 1% fetal calf serum and 50 mg/liter penicillin-streptomycin; 4 ml per 10-cm dish). After 24 h of incubation, the culture medium was aspirated and centrifuged at 2,000 × *g*. The supernatant was directly used for immunoblot analysis. For α-Pcdh PS-IP experiments with SH-SY5Y cells and primary neuronal culture, the γ-secretase inhibitor DAPT {*N*-[*N*-(3,5-difluorophenacetyl)-L-alanyl]-(*S*)-phenylglycine*t*-butyl ester} (7.5 μM; Calbiochem) and the MMP inhibitor TAPI-1 [*N*-(*R*)-(2-(hydroxyaminocarbonyl)methyl)-4-methylpentanoyl-L-naphthylalanyl-L-alanine 2-aminoethyl amide] (40 μM; Calbiochem) were added 12 h after the change to fresh medium, and cells were harvested after an additional incubation for 12 h. The proteasome inhibitor lactacystin (5 μM; Sigma) and the Golgi apparatus disintegrating reagent brefeldin A (BFA) (36 μM; Sigma) were supplied with fresh medium, and cells were harvested 24 h later.

Neuronal culture and virus infection. Dissociated cortical neurons of rats and of γ-*Pcdh*$^{+/+}$, γ-*Pcdh*$^{+/-}$, γ-*Pcdh*$^{-/-}$ mice (11) were plated at a density of 10^7 cells/10-cm dish for surface biotinylation experiments, and crude protein extracts were plated at a density of 10^5 cells/coverslip in 12-well plates for immunocytochemistry. Neurons were infected with recombinant adeno-associated virus (rAAV) or lentivirus at 2 days in vitro (DIV 2) and were harvested at DIV 14 (10-cm dishes) or DIV 21 (12-well plates with coverslips). For the generation of infectious rAAV expressing myc-Pcdhα4, myc-PcdhγAI, or myc-α-constant domain (CD) (Table 1), HEK293 cells were transfected with the respective pAAV and helper plasmids by the calcium phosphate method and grown for 2 days (7, 37). After being washed twice with phosphate-buffered saline (PBS), cells were lysed by three repeated freeze-thaw cycles and centrifuged at 2,000 × *g*, and the virus-containing supernatant was taken for infection experiments. Viral titers (~10^6 particles/μl) were determined by titration of the virus on rat primary

hippocampal cultures and counting of the infected cells (determined by staining with respective antibodies [Ab]). Lentiviruses were produced as described previously (19, 23). In brief, human embryonic kidney 293FT cells (Invitrogen) were transfected by the calcium phosphate method with expression plasmid and two helper plasmids (Δ8.9 and vesicular stomatitis virus G protein) (26, 52). After 48 h, the supernatants from four 10-cm dishes were pooled, centrifuged at 780 × *g* for 5 min, filtered with a 0.45-μm-pore-size filter (Nalgene), and centrifuged at 83,000 × *g* for 1.5 h. Pellets were resuspended in 100 μl of PBS, pH 7.2.

Surface biotinylation assay and PSD preparation. Murine cortical neuronal cultures at DIV 14 were washed twice with PBS and subsequently surface biotinylated with 1 mg/ml Sulfo-NHS-SS-Biotin [sulfosuccinimidyl 2-(biotinamido)-ethyl-1,3-dithiopropionate; Pierce] at 4°C for 30 min. After the neurons were washed three times with PBS, cells were lysed in lysis buffer (20 mM sodium phosphate [pH 7.5], 150 mM NaCl, 0.1% sodium dodecyl sulfate, 0.5% NP-40, 0.5% sodium deoxycholate, Complete Protease Inhibitor [Roche]). Biotinylated proteins were isolated with NeutrAvidine beads as described by the manufacturer (Pierce). Postsynaptic density (PSD)-enriched fractions of mouse brain were prepared as described previously (38).

MMP siRNA. Transfection of 21-nucleotide small interfering RNA (siRNA) duplexes (MWG) for silencing endogenous genes was carried out with Lipofectamine 2000 according to the manufacturer's protocol (Invitrogen). The highest efficiencies in silencing specific genes were obtained by using mixtures of siRNA duplexes targeting different regions of the gene of interest. Sequences of siRNAs used were 5′-AAUGAAGAGGGACACUUCCCUdTdT-3′ and 5′-AAGUUGCCUCCUCCUAAACCAdTdT-3′ (ADAM10); 5′-AACUCCAUCUGUUCUCCUGACdTdT-3′ and 5′-AAAUUGCCAGCUGCGCCCGUCdTdT-3′ (ADAM15); and 5′-AAAGUUUGCUUGCACACCUUdTdT-3′, 5′-AAGUAAGGCCCAGGAGUGUUdTdT-3′, and 5′-AACAUAGAGCCACUUUGGAGAdTdT-3′ (ADAM17) (5, 8). BlockIt (Invitrogen) was used as the control siRNA.

Constructs. All cDNA inserts subcloned into vectors for transient transfections in cell lines were generated by reverse transcriptase (RT)-PCR from RNA of neonatal rat brains. All cloned inserts for cell transfection were sequenced. In brief, total RNA isolated from rat brain with TRI Reagent (Molecular Research Center) was reverse transcribed (Moloney murine leukemia virus reverse transcriptase; Invitrogen) using random hexamer primers. Enzymes were heat inactivated after RNase H (USB) treatment. pRK5-myc-α-CD was generated as described previously (11). pRK5-yellow fluorescent protein (YFP)-PcdhγA1 was constructed by RT-PCR using the primer pair A1vr5 (5′-GCCCTAGGGGAAACATCCGATACTCTGTGCC-3′) and A1vr3 (5′-GTCCTAGGTTACTTCTTCTCTTTCTCGCC-3′). The resulting ~2.8-kb DNA fragment was cloned into the XbaI restriction site of ΔRK5-mycCP3-YFP (11). All green fluorescent protein (GFP) variants used were enhanced fluorescent proteins (enhanced YFP [eYFP], enhanced cyan fluorescent protein [eCFP], and eGFP). pRK5 CFP-Pcdhα4 was generated in the same manner by RT-PCR using the primer pair CNR1STOP/Xba (5′-GCTCTAGATCACTGGTCACTGTTGTCCGTCGT-3′) and CNR1-Xba (5′-GCTCTAGAGGGAACAGCCAGATCCACTACTCC-3′), cloning the resulting ~2.8-kb fragment into the XbaI restriction site of ΔRK5-mycCP3-CFP. The plasmid pRK5-CP3myc-Pcdhα4 was constructed by generating a 159-bp PCR fragment with KOD polymerase (Novagen) from the template vector ΔRK5-mycCP3-CFP (11) with the primer pair CP3_mF_for (5′-AATGGATCCACCATGTTCAAGATCCTGCTGGTC-3′) and CP3_mF_rev (5′-ATAAAGCTTATTTCTAGACTTATCGTCGTCATCCTTGTAATCCATAGCAGCAGCCAGGTCCTCCTCGGAGATCAGC-3′) and inserting it into the BamHI/HindIII restriction sites of pRK5, thus creating pRK5-CP3myc. PCR with the template vector pRK5-CFP-Pcdhα4 and the primer pair alpha4_CP3_for (5′-TTAGGATCCACCATGTTCAAGATCCTGCTGGTCTG-3′) and alpha4_rev (5′-TTAAAGCTTTCACTGGTCACTGTTGTCCGTCG-3′) resulted in a ~2.8-kb DNA fragment, which was inserted into the XbaI restriction site of pRK5-CP3myc, thus constructing pRK5-CP3myc-Pcdhα4. The plasmid pRK5-CP3myc-PcdhγA1 was generated in the same manner. PCR using the template pRK5-CFP-PcdhγA1 and the primer pair FLAGgAI_for (5′-TTACCTAGGAACATCCGATACTCTGTGCCAGAAG-3′) and FLAGgAI_rev (5′-TTACCTAGGTTACTTCTTCTCTTTCTTGCCCG-3′) resulted in a ~2.7-kb DNA fragment, which was inserted into the XbaI restriction site of pRK5-CP3myc. pAAV-Syn-myc-PcdhγAI was constructed by restricting pRK5-CP3myc-PcdhγAI with BamHI and HindIII and inserting the resulting CP3myc-PcdhγAI fragment (~2.8 kb) into pAAV-6P-SEWB (7, 37), linearized with the same enzymes. pAAV-Syn-myc-Pcdhα4 was constructed accordingly. The plasmid pAAV-Syn-myc-α-CD was constructed by generating a 543-bp PCR fragment with the template vector pRK5-myc-α-CD and the primer pair agICD_for (5′-CGAAGATCTAACATGGAGGAGCAGAAGCTGATCTC-3′) and aICD_rev (5′-CTCAGATCTTCATCACTGGTCACTGTTGTCCGTC-3′) and inserting it into the BamHI restriction site of pAAV-Syn-Venus. pLenti-α-siRNA-eGFP was generated by cloning double-stranded hairpin oligonucleotide (5′-TTTGAACAGCACGACGGACAACAGGTGAAGCCACAGATGCTGTTGTCCGTCGTGCTGTTCTTTTT-3′) targeting the C-terminal constant region of murine α-Pcdhs via its BstBI/BbsI restriction sites into pCMV-U6 (2). Subsequently, the U6-α-siRNA cassette was subcloned via its NheI/BstBI restriction sites into FUGW, including a NheI/BstBI linker (2), creating pLenti-α-siRNA-eGFP. pLenti-GFP-siRNA was constructed accordingly, with a GFP-targeting sequence (42).

Immunoblotting, immunocytochemistry, and Ab. Mouse brain extracts were prepared as described previously (11). For preparation of crude protein extracts of cultured cells, cells were washed twice with PBS and lysed in lysis buffer (25 mM HEPES [pH 7.4], 150 mM NaCl, 0.5% TX-100, Complete Protease Inhibitor [Roche]). Following a 10-min incubation, the lysate was centrifuged, and the supernatant was taken for further analysis. Lysates or immunoprecipitated (IPr) proteins were separated by sodium dodecyl sulfate-polyacrylamide gel electrophoresis on 10% gels under standard conditions (32) and transferred onto polyvinylidene difluoride membranes (0.45 μm; Amersham). Reactive bands were labeled using the following primary Ab: mouse anti-NR1 (1:2,000; Chemicon), rabbit anti-ADAM10 (1:1,000; Chemicon), rabbit anti-ADAM15 (1:1,000; Chemicon), rabbit anti-ADAM17 (1:1,000; Chemicon), mouse anti-myc (1:1,000; Sigma), rabbit anti-GFP (1:5,000; Abcam), and mouse anti-β-actin (1:10,000; Abcam). Rabbit polyclonal antiserum against γ-Pcdhs (1:1,000) was generated by Eurogentech Laboratories from purified soluble γ-ICD-10his protein as described previously (11). Rabbit polyclonal antiserum detecting amino acids 879 to 947 (numbered according to the Pcdhα4/CNRI sequence) of the C-terminal α-Pcdh constant region was generated by GENOVAC. After incubation with peroxidase-coupled anti-rabbit/anti-mouse Ab (Amersham Biosciences), the blots were developed with chemiluminescent reagents (Pierce). Films of immunoblots were scanned with a flatbed scanner, and digital images were imported and processed by Photoshop software (Adobe). Quantification of immunoblots was performed with ImageJ software. Immunocytochemistry was performed by standard protocols. Briefly, 10^5 cells were seeded on 18-mm poly-L-lysine-coated glass coverslips and transfected 24 h later. Staining was 48 h after transfection, either under permeabilizing conditions or under nonpermeabilizing conditions without Triton X-100 (surface/live staining). Primary Ab dilutions were 1:200, and species-specific secondary Ab were conjugated with fluorescein isothiocyanate or Cy3 (Jackson ImmunoResearch; 1:500). Coverslips were mounted on slides with Mowiol embedding medium (KSE).

Fluorescence microscopy and imaging. Detection of fluorescence in cells grown on coverslips was conducted by confocal laser scanning microscopy with a Zeiss LSM5 Pa microscope. Surface mean intensity, mean area, and mean number of puncta per 20-μm secondary/tertiary dendrite of live stained neurons were analyzed using WCIF ImageJ.

RESULTS

α-Pcdh processing. We first determined if α-Pcdhs undergo membrane processing similar to that undergone by γ-Pcdhs (9, 11) (Fig. 1A). Of the 14 different α-isoforms, we selected Pcdhα4/CNR1 and constructed a vector expressing this isoform as an N-terminal fusion to CFP (CFP-Pcdhα4) (Table 1). Since α-Pcdhs are expressed predominantly in neurons, we expressed CFP-Pcdhα4 in SH-SY5Y cells, a homogenous, readily transfectable neuroblastoma cell line. As controls for our Ab, we expressed myc-PcdhγAI in SH-SY5Y cells. Crude cellular protein lysates of SH-SY5Y cells transiently expressing myc-PcdhγAI (Fig. 1B, lane 1) or CFP-Pcdhα4 (lane 2) were subjected to immunoblot analysis with our Ab directed against the C-terminal constant part of α-Pcdhs (anti-Cα). Cα Ab detected a band of approximately 130 kDa, representing full-length CFP-Pcdhα4 (CFP-α4) fusion protein, and a smaller band of approximately 30 kDa, having the expected size of a juxtamembrane cleavage product (α4-CTF-1) (Fig. 1B, lane 2), suggesting intramembrane proteolysis of α-Pcdhs. Consistently, we found shedded ectodomain of CFP-Pcdhα4 (α4 extracellular domain [α4-ECD]) only in the culture medium of CFP-Pcdhα4-expressing cells probed with anti-GFP Ab (Fig. 1B, upper panel). To determine Cγ Ab specificity, we tran-

siently expressed CFP-Pcdhα4 or myc-PcdhγAI in SH-SY5Y cells (Fig. 1C, left panel). Immunoblot analysis with Cγ Ab detected bands representing full-length myc-PcdhγAI (~100 kDa) and the cleavage product (γAI-CTF-1, ~30 kDa) in lysates of SH-SY5Y cells expressing myc-PcdhγAI (Fig. 1C, lane 1) and not in lysates of cells expressing CFP-Pcdhα4 (lane 2). Additional immunoblot analyses of crude mouse brain lysates of P0 γ-Pcdh wild-type (*Pcdhγ*$^{+/+}$) (Fig. 1C, lane 3) or knockout (*Pcdhγ*$^{-/-}$) (lane 4) mice with Cγ Ab detected bands representing endogenous full-length γ-Pcdh (~100 kDa) and γ-CTF1 (~30 kDa) only in *Pcdhγ*$^{+/+}$ lysates. These results suggested PS-IP of α-Pcdhs in SH-SY5Y cells, reminiscent of γ-Pcdh PS-IP (9, 11).

MMP and γ-secretase cleavage of Pcdhα4. The defining feature of PS-IP is successive cleavage of the substrate by an MMP and the γ-secretase complex. To assess the role of MMPs and γ-secretase in α-Pcdh processing, we treated SH-SY5Y cells transiently expressing CFP-Pcdhα4 with the pan-MMP inhibitor TAPI-1 or the specific γ-secretase inhibitor DAPT (Fig. 1A). As a positive control, we monitored the generation of the γAI-CTF-1 fragment in YFP-PcdhγAI-expressing cells (immunoblot not shown) (9, 11). Inhibition of MMP-mediated ectodomain shedding with TAPI-1 should decrease the amount of the cytoplasmic membrane-bound cleavage intermediate (α4-CTF-1, ~30 kDa) and increase the amount of the full-length protein (CFP-α4, 131 kDa). Conversely, treatment with DAPT should increase the amount of the 30-kDa α4-CTF-1, due to inhibition of the γ-secretase complex. Indeed, immunoblot analysis with anti-Cα Ab showed a reduction of the band corresponding to the 30-kDa α4-CTF-1 when treated with TAPI-1 (Fig. 2A, lane 2) and an accumulation of α4-CTF-1 when treated with DAPT (lane 3), compared to the control treatment with dimethyl sulfoxide (DMSO) (lane 1). Figure 2B summarizes the results of α-Pcdh cleavage, showing α4- and γAI-Pcdh CTF-1 protein levels for DMSO (control), TAPI-1, and DAPT treatment. There was a reduction to ~50% ($P < 0.01$) in α4- and γAI-Pcdh CTF-1 generation upon TAPI-1 treatment and an increase to ~200% ($P < 0.01$) upon DAPT treatment, compared to control levels (DMSO treatment). These results indicate involvement of MMPs and the γ-secretase complex in the proteolysis of α-Pcdhs.

Processing of the 30-kDa α4-CTF-1 by the γ-secretase complex should result in the generation of a ~26-kDa α4-CTF-2 (Fig. 1A), but we could detect a faint band of the expected size only upon prolonged exposure of the immunoblots shown in Fig. 1B and Fig. 2A. The CTF-2 of γ-Pcdhs is rapidly degraded by the proteasome complex (9). To prevent degradation of the soluble α4-CTF-2, we made use of the proteasome inhibitor lactacystin (4). Lactacystin treatment of untransfected SH-SY5Y cells (Fig. 2C, lane 1) or DMSO treatment of transiently CFP-Pcdhα4-expressing SH-SY5Y cells revealed a faint, ~26-kDa α4-CTF-2 immunoreactive band, whereas lactacystin treatment of SH-SY5Y cells transiently expressing CFP-Pcdhα4 (lane 3) robustly increased the intensity of the ~26-kDa α4-CTF-2 band.

To further substantiate the processing of α-Pcdhs by the γ-secretase complex, we transiently transfected presenilin1/2 dko mouse embryonic fibroblasts (13, 14) to express CFP-Pcdhα4 and treated them with lactacystin. A subsequent immunoblot analysis with the anti-Cα Ab revealed substantial

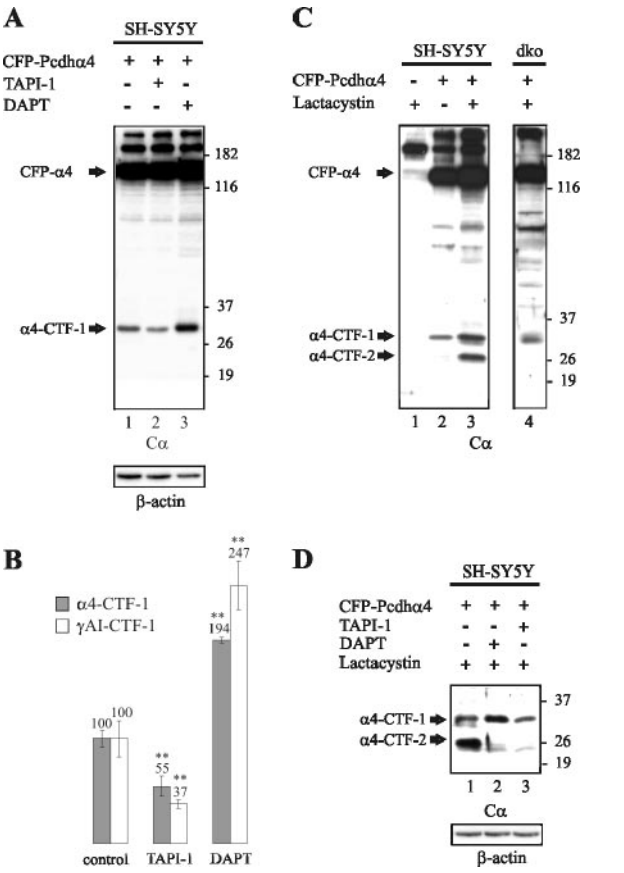

FIG. 2. Sequential MMP and γ-secretase cleavage of CFP-Pcdhα4 in SH-SY5Y cells. (A) Upper panel, immunoblot with anti-Cα Ab (Cα) of whole-cell lysates of SH-SY5Y cells transiently expressing CFP-Pcdhα4 and treated with DMSO (lane 1), TAPI-1(lane 2), or DAPT (lane 3). Arrows indicate the immunoreactive bands for CFP-Pcdhα4 (131 kDa; CFP-α4) (molecular mass markers [in kilodaltons] are shown on the right) and α4-CTF-1 (~30 kDa). Lower panel, immunoblot of the lysates with anti-β-actin Ab (β-actin) serving as the loading control. Above the immunoblots is a scheme for the expression of CFP-Pcdhα4 and treatment with TAPI-1 or DAPT in SH-SY5Y cells. (B) Quantification of results shown in panel A for α4-CTF-1 levels compared to β-actin and, as a positive control, for γAI-CTF-1 levels in transiently YFP-PcdhγAI-expressing SH-SY5Y cells, treated with DMSO, TAPI-1, or DAPT (as percentages of the control; $n = 4$). The bar graph includes the average values ± standard errors of the means (SEM), and significant differences (**, $P \leq 0.01$ by ANOVA) between control (DMSO) and treatment (TAPI-1 or DAPT) conditions are indicated. (C) Immunoblot with anti-Cα Ab (Cα) of SH-SY5Y and presenilin dko cells transiently expressing CFP-Pcdhα4 (lanes 2 to 4), treated with either DMSO (lane 2) or lactacystin (lanes 1, 3, and 4). Arrows indicate the immunoreactive band for CFP-Pcdhα4 (CFP-α4) and the corresponding α4-CTF-1 and α4-CTF-2 (~26-kDa) bands. The scheme above the immunoblots shows the expression of CFP-Pcdhα4 and lactacystin treatment of SH-SY5Y cells. (D) Upper panel, immunoblot with anti-Cα Ab (Cα) of SH-SY5Y cells transiently expressing CFP-Pcdhα4 (lanes 1 to 3) and treated with lactacystin (lanes 1 to 3) and either DAPT (lane 2) or TAPI-1 (lane 3). Lower panel, immunoblot of corresponding lysates with anti-β-actin Ab (β-actin) serving as the loading control. Above the immunoblots is a scheme representing the expression of CFP-Pcdhα4 and lactacystin, DAPT, or TAPI-1 treatment of SH-SY5Y cells.

immunoreactivity of the presumptive membrane-bound 30-kDa α4-CTF-1 and the absence of the 26-kDa α4-CTF-2 (Fig. 2C, lane 4).

Finally, we assessed the amount of α4-CTF-2 in lysates of SH-SY5Y cells overexpressing CFP-Pcdhα4 that had been treated with lactacystin and TAPI-1 or lactacystin and DAPT (Fig. 2D). The strong α4-CTF-2 immunoreactivity upon lactacystin treatment alone (lane 1) and weak α4-CTF-2 immunoreactivity upon lactacystin/DAPT (lane 2) or lactacystin/TAPI-1 treatment (lane 3) are in accordance with the assumption that α4-CTF-2 represents a product of γ-secretase-mediated α4-CTF-1 cleavage. This demonstrates sequential MMP- and γ-secretase-mediated cleavage of CFP-Pcdhα4 in SH-SY5Y cells, the former generating α4-CTF-1 and the latter α4-CTF-2.

ADAM10-dependent ectodomain shedding of Pcdhα4. The initial step in intramembrane proteolysis of α/γ-Pcdhs seems to be the cleavage of the substrate by an MMP. The nature of the MMP determines the conditions and therefore the regulation of the intramembrane proteolysis. The fact that substrates for PS-IP, such as classical cadherins and γ-Pcdhs, are cleaved by similar proteases suggested that a member of the ADAM family might be responsible for ectodomain shedding. Therefore, we cotransfected SH-SY5Y cells with siRNAs targeting ADAM10, -15, or -17 (5, 8) and plasmid expressing CFP-Pcdhα4 and visualized immunoreactive bands by immunoblot analysis (Fig. 3A). Unspecific siRNA (BlockIt; Invitrogen) (referred to hereafter as "control siRNA") served as the negative control. Treatment of the cells with siRNA for ADAM10, -15, or -17 resulted in a marked decrease in the intensities of the immunoreactive bands of the respective MMPs (Fig. 3A, upper panels, lanes 2 to 4), validating the silencing approach. The immunoblot probed with anti-Cα Ab showed a reduction to 29% of control levels in the intensity of α4-CTF-1 only in the α-ADAM10 siRNA-cotransfected cells (Fig. 3A, lane 2; Fig. 3B), whereas α-ADAM15, α-ADAM17, and control siRNAs had no obvious effects on the amount of the α4-CTF-1 (Fig. 3A and B). In accordance, we detected a marked increase in the intensity of the immunoreactive band corresponding to the full-length CFP-Pcdhα4 (CFP-α4) only in the α-ADAM10 siRNA-treated cells, whereas the levels of CFP-α4 in α-ADAM15 or α-ADAM17 siRNA-treated cells stayed unchanged compared to control levels.

This result suggests that in SH-SY5Y cells ADAM10 affects shedding of Pcdhα4, similar to the ADAM10-dependent cleavage of PcdhγC3 and N-cadherin in neurons (21, 30).

Altered cleavage of α- and γ-Pcdh heteromers in SH-SY5Y cells. α- and γ-Pcdhs form homo- and heteromers (24). Due to the different susceptibilities of the isoforms to MMP cleavage and PS-IP (9), the formation of α- and γ-Pcdh homo- and heteromers may create receptors with distinct turnover/signaling. To investigate if the expression of α-Pcdhs could influence the presenilin-dependent processing of γ-Pcdhs, we transfected SH-SY5Y cells with vectors expressing YFP-PcdhγAI or YFP-PcdhγAI/myc-Pcdhα4. To visualize the localization of PcdhγAI, we performed live staining with anti-GFP Ab of cells expressing either YFP-PcdhγAI or YFP-PcdhγAI/myc-Pcdhα4 (Fig. 4A and B). Although we could not detect a significant difference in surface expression of YFP-PcdhγAI in SH-SY5Y cells transiently expressing YFP-PcdhγAI or YFP-PcdhγAI/myc-Pcdhα4 (Fig. 4A and B), we found an increase in intracellular YFP fluorescence in cells coexpressing YFP-PcdhγAI/myc-Pcdhα4 (Fig. 4A and B). To assess if the internal accumulation of YFP-PcdhγAI resulted from reduced turnover of Pcdhs at the cell surface, we performed immunoblot analysis (Fig. 4C). SH-SY5Y cells coexpressing YFP-PcdhγAI/myc-Pcdhα4 showed a twofold increase in full-length YFP-PcdhγAI (Fig. 4C and D, CFP-γAI) and a sevenfold decrease in γAI-CTF-1 amounts, compared to levels in cells expressing only YFP-PcdhγAI. One explanation for the reduced turnover of PcdhγAI upon coexpression of Pcdhα4 is heteromer formation.

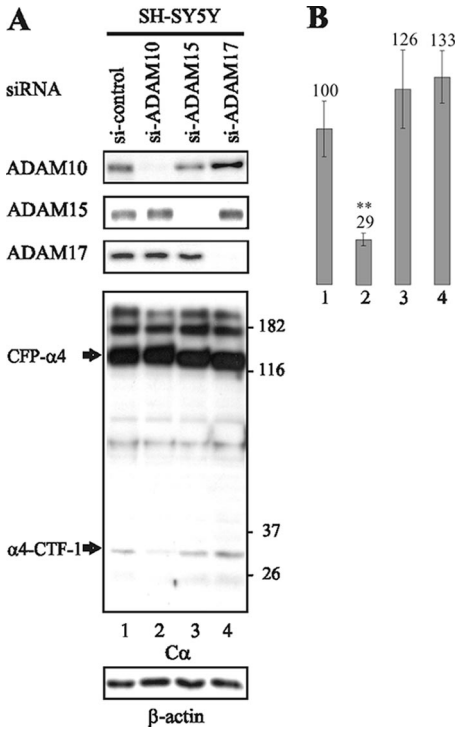

FIG. 3. ADAM10 cleavage of Pcdhα4. (A) Immunoblot with anti-ADAM10, -15, and -17 and anti-Cα and -β-actin Ab of whole-cell protein lysate of SH-SY5Y cells transiently expressing CFP-Pcdhα4 and cotransfected with different siRNAs (lane 1, si control; lane 2, si-ADAM10; lane 3, si-ADAM15; lane 4, si-ADAM17). Arrows indicate the immunoreactive bands for CFP-Pcdhα4 (CFP-α4; 131 kDa) (molecular mass markers [in kilodaltons] are shown on the right) and its corresponding α4-CTF-1 (~30 kDa). (B) Quantification of results shown in panel A. The bar graph includes the average values ± SEM, and significant differences (**, $P \leq 0.01$ by ANOVA) for quantifying changes in α4-CTF-1 levels compared to β-actin (as percentages of the control; $n = 3$) are indicated.

To determine the effect of γ-Pcdh expression on α-Pcdh cleavage, we transfected SH-SY5Y cells with vectors expressing CFP-Pcdhα4 or CFP-Pcdhα4/myc-PcdhγAI. Live staining with anti-GFP Ab (Fig. 4E and F) revealed a marked increase of CFP-Pcdhα4 surface delivery and a concomitant decrease of direct intracellular CFP fluorescence upon coexpression of CFP-Pcdhα4/myc-PcdhγAI compared to expression of CFP-Pcdhα4 alone. These results are in accordance with those from a previous study showing γ-Pcdh-dependent surface delivery of α-Pcdhs in heterologous cell systems (24). Immunoblot analysis with an anti-Cα Ab of protein lysates of SH-SY5Y cells

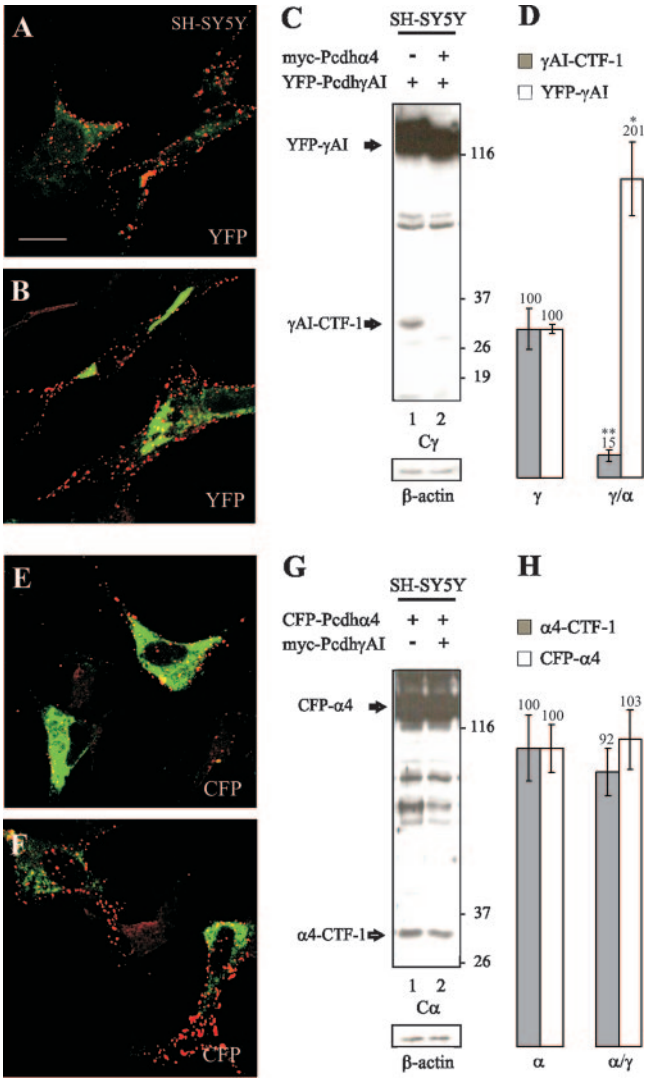

FIG. 4. Effects of Pcdhα4 on PcdhγAI cleavage in SH-SY5Y cells. (A and B) Surface immunocytochemistry with anti-GFP Ab (red) of SH-SY5Y cells transiently expressing YFP-PcdhγAI (A) or coexpressing YFP-PcdhγAI/myc-Pcdhα4 (B) (scale bar = 10 μm). Direct YFP fluorescence is shown in green (YFP). (C) Upper panel, immunoblot with anti-Cγ Ab (Cγ) of protein lysates of SH-SY5Y cells transiently expressing either YFP-PcdhγAI (lane 1) or coexpressing YFP-PcdhγAI/myc-Pcdhα4 (lane 2). Arrows mark immunoreactive bands corresponding to YFP-PcdhγAI (YFP-γAI; ~130 kDa) (molecular mass markers [in kilodaltons] are shown on the right) and γAI-CTF-1 (~30 kDa). Lower panel, immunoblot of corresponding lysates with anti-β-actin Ab (β-actin) serving as the loading control. The scheme above the immunoblots shows the expression of YFP-PcdhγAI and myc-Pcdhα4 in SH-SY5Y cells. (D) Quantification of results shown in panel C. The bar graph includes the average values ± SEM, and significant differences (**, $P \leq 0.01$ by *t* test) quantifying changes in γAI-CTF-1 and YFP-γAI levels compared to β-actin (as percentages of the amounts in YFP-PcdhγAI-expressing cells; $n = 4$) are indicated. (E and F) Surface immunocytochemistry with anti-GFP Ab (red) of SH-SY5Y cells transiently expressing CFP-Pcdhα4 (E) or coexpressing CFP-Pcdhα4/myc-PcdhγAI (F). Direct CFP fluorescence is shown in green (CFP). (G) Upper panel, immunoblot with anti-Cα Ab (Cα) of protein lysates of SH-SY5Y cells transiently expressing either CFP-Pcdhα4 (lane 1) or coexpressing CFP-Pcdhα4/myc-PcdhγAI (lane 2). Arrows mark immunoreactive bands corresponding to CFP-Pcdhα4 (CFP-α4; ~130 kDa) and α4-CTF-1 (~30 kDa). Lower panel, immunoblot of corresponding lysates with anti-β-actin Ab (β-actin) serving as the loading control. Above the immunoblots is a scheme representing the expression of CFP-Pcdhα4 and myc-PcdhγAI in SH-SY5Y cells. (H) Quantification of results shown in panel G. The bar graph includes the average values ± SEM, and significant differences (**, $P \leq 0.01$ by *t* test) quantifying changes in α4-CTF-1 and CFP-α4 levels compared to β-actin (as percentages of the amounts in CFP-Pcdhα4-expressing cells; $n = 4$) are indicated.

expressing CFP-Pcdhα4 or CFP-Pcdhα4/myc-PcdhγAI yielded significant differences for neither full-length CFP-Pcdhα4 levels nor α4-CTF-1 levels (Fig. 4G and H). Thus, in spite of increased surface delivery of CFP-Pcdhα4 upon coexpression of myc-PcdhγAI, we did not observe increased generation of α4-CTF-1. One explanation might be altered susceptibility of α/γ-Pcdh heteromers to PS-IP.

PS-IP of Pcdhα4 in neurons. α-Pcdhs appear to be confined largely to the CNS (17). Since SH-SY5Y cell systems lack prominent neuronal characteristics, including axons, dendrites, and synapses, they may not faithfully represent in vivo α-Pcdh processing. To assess if PS-IP, as seen for Pcdhα4 in SH-SY5Y cells, also takes place in cultured primary cortical neurons, we infected such cultures with rAAV expressing myc-Pcdhα4 (or myc-PcdhγAI) (Table 1) and treated them with DMSO, TAPI-1, DAPT, or lactacystin. Overexpression of myc-Pcdhα4 in neurons expressing endogenous α-Pcdh was necessary due to the many unspecific bands detected by the anti-Cα Ab. Since extensive overexpression of myc-Pcdhα4 in cultured neurons could lead to nonphysiological localization and cleavage of the protein, we first monitored proper localization of the overexpressed myc-Pcdhα4 and assessed the amount of rAAV-mediated myc-Pcdhα4 expression relative to endogenous α-Pcdh levels. To visualize the localization of overexpressed myc-Pcdhα4 and endogenous γ-Pcdh, we costained myc-Pcdhα4-expressing neurons with an anti-myc Ab under nonpermeabilizing conditions and with an anti-Cγ Ab (11) under permeabilizing conditions. As shown in Fig. 5A, overexpressed myc-Pcdhα4 and endogenous γ-Pcdh colocalize to dendrites in discrete puncta, reminiscent of endogenous α- and γ-Pcdh distribution (24). To estimate the level of myc-Pcdhα4 overexpression, we analyzed crude protein lysates of primary cortical cultures that were either naive (Fig. 5B, lane 1) or infected with rAAV expressing myc-Pcdhα4 (lane 2) by immunoblotting with anti-Cα Ab. The overexpression of myc-Pcdhα4 increased the amount of total α-Pcdh fourfold (Fig. 5C, bars 1 and 2). In analogy, we compared the levels of endogenous γ-Pcdh expression (lane 3) to levels of overexpression of myc-PcdhγAI (lane 4). Overexpression of myc-PcdhγAI increased total γ-Pcdh levels nearly sevenfold (Fig. 5C, bars 3 and 4).

Finally, we analyzed protein lysates of primary cultures on immunoblots with anti-Cα Ab and detected identical MMP- and γ-secretase-dependent cleavage of myc-Pcdhα4 (and myc-PcdhγAI) shown for SH-SY5Y cells (Fig. 5D; data for myc-PcdhγAI not shown). TAPI-1 decreased and DAPT increased the immunoreactive band corresponding to α4-CTF-1. Treatment with lactacystin increased the intensity of the α4-CTF-2 immunoreactive band. These results substantiate MMP and γ-secretase cleavage of Pcdhα4 in neurons. Interestingly, the PS-IP of myc-Pcdhα4 seemed to be less efficient than that of

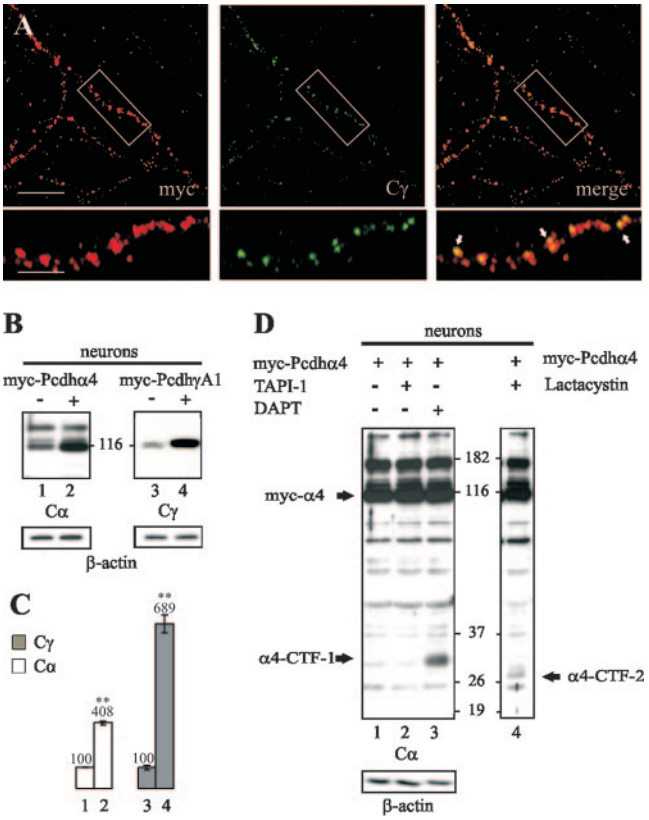

FIG. 5. MMP and γ-secretase cleavage of myc-Pcdhα4 in primary neurons. (A) Colocalization of overexpressed myc-Pcdhα4 and endogenous, cellular γ-Pcdh. Upper panels, surface immunocytochemistry with anti-myc Ab (myc; red) and cellular immunocytochemistry with anti-Cγ Ab (Cγ; green) of DIV 21 primary hippocampal cultures infected with rAAV expressing myc-Pcdhα4 (scale bar = 10 μm). Colocalization of surface myc-Pcdhα4 and cellular γ-Pcdh is shown in yellow (merge). Lower panels, higher-magnification pictures of the insets in the upper panels (scale bar = 3 μm; arrows indicate selected yellow puncta). (B) Left upper panel, immunoblot analysis with anti-Cα Ab (Cα) of protein lysates of DIV 14 rat primary cortical cultures, either uninfected (control neurons, lane 1) or infected with rAAV expressing myc-Pcdhα4 (lane 2). Right upper panel, immunoblot analysis with anti-Cγ Ab of rat cortical neurons, either uninfected (control neurons, lane 3) or infected with rAAV expressing myc-PcdhγAI (lane 4). A molecular mass marker (in kilodaltons) is shown between left and right upper panels. Right and left lower panels, immunoblots of corresponding lysates with anti-β-actin Ab (β-actin) serving as the loading controls. The scheme above the immunoblots represents the expression of myc-Pcdhα4 and myc-PcdhγAI in neurons. (C) Quantification of results shown in panel B. The bar graph includes the average values ± SEM, and significant differences (**, $P \leq 0.01$ by t test) for full-length α- and γ-Pcdhs between uninfected and infected neurons (as percentages of endogenous α/γ-Pcdh levels; $n = 4$) are indicated. (D) Upper panel, immunoblot analysis with anti-Cα Ab (Cα) of DIV 14 primary cortical cultures infected with rAAV expressing myc-Pcdhα4. For treatments, see the scheme above the immunoblot. Arrows indicate the immunoreactive bands for myc-Pcdhα4 (myc-α4; 100 kDa) and its corresponding α4-CTF-1 and α4-CTF-2 (~26 kDa). Lower panel, immunoblot of corresponding lysates with anti-β-actin Ab (β-actin) serving as the loading control.

myc-PcdhγA1, as estimated by the steady-state ratios of the α- and γ-Pcdh full-length proteins to their CTF-1s (data not shown). This result is in analogy to differences in presenilin-dependent processing between different γ-Pcdh isoforms (9).

As most receptors require surface delivery prior to PS-IP (e.g., N- and E-cadherins, γ-Pcdhs) (11, 20, 21), we determined the location of α-Pcdh cleavage by employing BFA, which disintegrates the Golgi apparatus and thereby suppresses surface delivery of membrane constituents (6). We infected rat primary cortical cultures with rAAV expressing myc-Pcdhα4 and treated them with BFA dissolved in DMSO or with DMSO alone for 12 h. Immunoblot analysis of protein lysates of BFA-treated neurons showed an ~85% reduction of the immunoreactive band corresponding to α4-CTF-1 compared to the levels with DMSO, providing an indication that α-Pcdhs are subject to PS-IP predominantly at the cell surface of neurons (data not shown).

Collectively, the data provide evidence of MMP and PS-IP cleavage of Pcdhα4 in the plasma membrane of neurons, with the first cleavage generating the membrane-tethered α4-CTF-1 and the second the soluble cytoplasmic α4-CTF-2.

α-Pcdh surface delivery in neurons is independent of γ-Pcdhs. Next, we sought to determine if α-Pcdh surface expression in neurons requires γ-Pcdhs as is the case in SH-SY5Y (see above) and other heterologous cell systems (24). To this end, cultured cortical neurons of wild-type (γ-*Pcdh*$^{+/+}$), heterozygous (γ-*Pcdh*$^{+/-}$), and knockout (γ-*Pcdh*$^{-/-}$) mice (11) were infected with rAAV expressing myc-Pcdhα4. After DIV 21, we performed live staining with anti-myc Ab to visualize surface-delivered myc-Pcdhα4 (Fig. 6A). Unexpectedly, γ-*Pcdh*$^{-/-}$ neurons showed substantial myc-Pcdhα4 surface levels, comparable to those in γ-*Pcdh*$^{+/+}$ and γ-*Pcdh*$^{+/-}$ neurons. To compare myc-Pcdhα4 surface delivery for the different genotypes, we counted puncta and measured the intensity and area per dendritic unit length (~20 μm). Although there was a slight reduction in the mean number of puncta in γ-*Pcdh*$^{-/-}$ neurons, we detected no significant differences in intensities, areas, or numbers of puncta for myc-Pcdhα4 surface expression among the different genetic backgrounds (Fig. 6B).

To corroborate these findings, we conducted a surface biotinylation assay. Cortical cultures of γ-*Pcdh*$^{+/+}$, γ-*Pcdh*$^{+/-}$, and γ-*Pcdh*$^{-/-}$ neurons were plated at high density and harvested at DIV 14. Quantification of the surface biotinylation was performed by immunoblot analysis (Fig. 6C). In the input fractions (Fig. 6C, lanes 1 to 3), the levels of full-length γ-Pcdh in γ-*Pcdh*$^{+/+}$, γ-*Pcdh*$^{+/-}$, and γ-*Pcdh*$^{-/-}$ neurons were 100%, ~36%, and 0%, respectively (quantified in Fig. 6D). Notably, α-Pcdh, NR1, and β-actin immunoreactive bands were unchanged. In the IPr fractions (Fig. 6C, lanes 4 to 6), γ-Pcdh surface protein levels were distributed in analogy to the γ-Pcdh input levels; compared to γ-Pcdh levels in γ-*Pcdh*$^{+/+}$ neurons (lane 4), γ-*Pcdh*$^{+/-}$ expressed ~35% (lane 5) and γ-*Pcdh*$^{-/-}$ 0% (lane 6). Again, there was a slight reduction in the amount of surface α-Pcdh in γ-*Pcdh*$^{-/-}$ neurons, but there were no significant differences for α-Pcdh or NR1 in the IPr fractions from γ-*Pcdh*$^{+/+}$, γ-*Pcdh*$^{+/-}$, or γ-*Pcdh*$^{-/-}$ neurons. We could not detect any β-actin immunoreactive bands in the IPr fractions, attesting to the integrity of our surface biotinylation. In summary, these results are consistent with the quantification by surface staining, indicating no statistically significant differences in surface delivery of α-Pcdhs in γ-*Pcdh*$^{+/+}$, γ-*Pcdh*$^{+/-}$, or γ-*Pcdh*$^{-/-}$ neurons.

We further investigated the abundance of synaptic α-Pcdh directly in mouse brain. We prepared postsynaptic density-

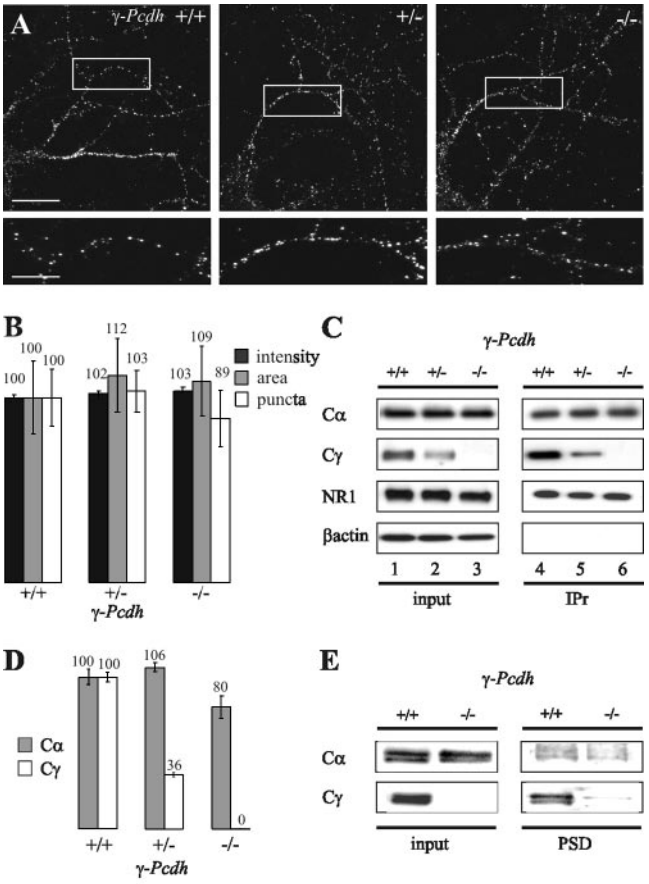

FIG. 6. Surface expression of myc-Pcdhα4 in γ-*Pcdh*$^{+/+}$, γ-*Pcdh*$^{+/-}$, and γ-*Pcdh*$^{-/-}$ neurons. (A) Upper panels, surface immunocytochemistry with anti-myc Ab of DIV 21 γ-*Pcdh*$^{+/+}$, γ-*Pcdh*$^{+/-}$, or γ-*Pcdh*$^{-/-}$ murine primary cortical cultures infected with rAAV expressing myc-Pcdhα4 (scale bar = 10 μm). Lower panels, higher magnification of the insets in the upper panels (scale bar = 3 μm). (B) Quantification of results shown in panel A. Bar graph of the surface mean intensities, mean areas, and mean numbers of puncta of myc-Pcdhα4 in γ-*Pcdh*$^{+/+}$, γ-*Pcdh*$^{+/-}$, or γ-*Pcdh*$^{-/-}$ neurons (as percentages of results for γ-*Pcdh*$^{+/+}$; dendrites of 12 different cells from three replicate experiments; $n = 12$). (C and D) Surface biotinylation of γ-Pcdh$^{+/+}$, γ-Pcdh$^{+/-}$, and γ-Pcdh$^{-/-}$ neurons. (C) Immunoblot analysis with anti-Cα, -Cγ, -NR1, and -β-actin Ab (Cα, Cγ, NR1, and βactin) of protein lysates of DIV 14 surface-biotinylated murine γ-*Pcdh*$^{+/+}$, γ-*Pcdh*$^{+/-}$, and γ-*Pcdh*$^{-/-}$ cortical primary cultures. Left panel (lanes 1 to 3), crude whole-cell lysate used as input for the IPr. Right panel (lanes 4 to 6), IPr of the surface-biotinylated proteins. (D) Quantification of results shown in panel C. Bar graph of α- and γ-Pcdh surface delivery normalized to NR1 surface delivery (as percentages of results for γ-*Pcdh*$^{+/+}$; $n = 4$). (E) Immunoblot analysis with anti-Cγ (Cγ) and anti-Cα (Cα) Ab of forebrain cellular (left panel) and PSD (right panel) protein fractions of P0 γ-*Pcdh*$^{+/+}$ and γ-*Pcdh*$^{-/-}$ mice.

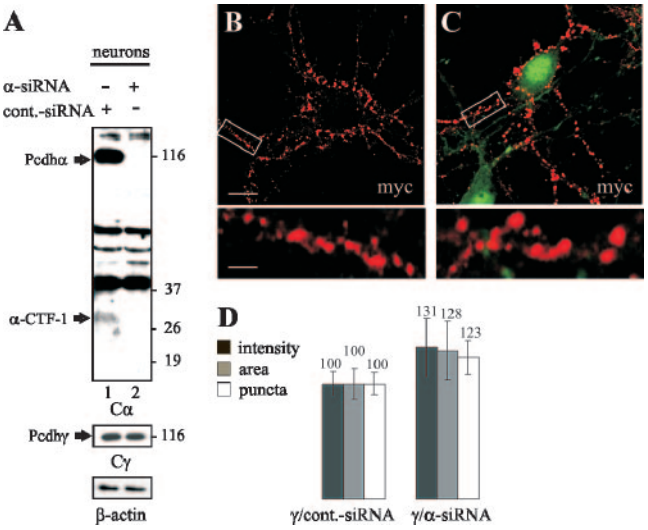

FIG. 7. α-siRNA and surface expression of myc-PcdhγAI in neurons. (A) Upper panel, immunoblot analysis with anti-Cα Ab of protein lysates of DIV14 murine primary cortical cultures infected with lentivirus expressing either GFP-siRNA (cont.-siRNA; lane 1) or α-siRNA (lane 2). Arrows indicate the immunoreactive bands for endogenous full-length α-Pcdh (Pcdhα) and α-CTF-1 as detected by Cα Ab (Cα) (molecular mass markers [in kilodaltons] are shown on the right). Middle panel, immunoblot analysis of full-length γ-Pcdh (Pcdhγ) with anti-Cγ Ab (Cγ) of lysates from panel A. Lower panel, immunoblot with β-actin Ab (β-actin) serving as the loading control. (B and C) Upper panels, surface immunocytochemistry with anti-myc Ab (myc) of murine primary cortical culture coinfected with rAAV expressing myc-PcdhγAI and lentivirus expressing either control siRNA (B) or α-siRNA (C) (scale bar = 10 μm). Direct GFP fluorescence is shown in green. Lower panels, higher magnification of the insets in the upper panels (scale bar = 2 μm). (D) Quantification of results shown in panel C. Bar graphs show the surface mean intensities, mean areas, and mean numbers of puncta of myc-PcdhγAI in neurons coexpressing myc-PcdhγAI and either control siRNA or α-siRNA ± SEM (as percentages of the amount in myc-PcdhγAI/control siRNA-expressing neurons; dendrites of seven different cells from three replicate experiments; $n = 7$).

enriched fractions (38) from forebrains of γ-*Pcdh*$^{+/+}$ and γ-*Pcdh*$^{-/-}$ mice and analyzed protein amounts of α-Pcdhs and γ-Pcdhs by immunoblot analysis (Fig. 6E). Again, there were no marked differences in the α-Pcdh protein levels among genotypes. In conclusion, it appears that, in cultured neurons and in vivo, α-Pcdh surface delivery is largely independent of γ-Pcdh expression.

To evaluate the influence of α-Pcdh expression on the cell surface expression of γ-Pcdhs in murine primary cortical culture, we designed a lentiviral construct expressing α-Pcdh-siRNA (α-siRNA) driven by the U6 promoter and Venus driven by the ubiquitin promoter. To monitor the downregulation of α-Pcdhs by α-siRNA, we infected mouse cortical neurons with virus expressing α-siRNA or GFP-siRNA (control siRNA) at DIV 2, harvested lysates at DIV 14, and analyzed immunoblots of protein lysates with anti-Cα, Cγ, and β-actin Ab (Fig. 7A). Infection with lentivirus expressing α-siRNA resulted in a robust decrease in full-length α-Pcdh immunoreactivity and presumptive α-CTF-1 (lane 2), compared to infection with control siRNA (lane 1) (or uninfected neurons; data not shown). Importantly, protein levels of γ-Pcdhs and β-actin were unchanged.

Moreover, we determined γ-Pcdh surface delivery in neuronal culture coexpressing by viral coinfection either myc-PcdhγAI/control siRNA or myc-PcdhγAI/α-siRNA (Fig. 7B and C). To visualize surface-delivered myc-PcdhγAI, we performed live stainings with anti-myc Ab. To determine the quantities of myc-PcdhγAI surface delivery for both conditions, we counted puncta and measured the intensity and area

per dendritic unit length (~20 μm). The slight increases in intensity (131%), area (128%), and the mean number of puncta (123%) in myc-PcdhγAI/α-siRNA-expressing neurons compared to myc-PcdhγAI/control siRNA-expressing neurons were not significant (by analysis of variance [ANOVA]) (Fig. 7D). The impact of α-Pcdh expression on γ-Pcdh surface delivery in rat primary neuronal culture is therefore minor, comparable to the situation in SH-SY5Y and HEK293 cells (24). Notably, α-siRNA- or control siRNA-expressing neurons exhibited neither gross morphological differences in dendritic branching or length nor increased cell death, as estimated by the number of viable infected cells compared to that of uninfected neurons (data not shown).

Altered α- and γ-Pcdh cleavage by heteromer formation in neurons. Next, we studied the effect of heteromer formation on α- and γ-Pcdh processing in rat primary neuronal culture. To investigate if the expression of Pcdhα4 influences the turnover of PcdhγAI, we coinfected rat primary cortical neurons with rAAVs expressing myc-PcdhγAI and either GFP or myc-Pcdhα4 and analyzed the abundance of full-length myc-PcdhγAI (myc-γAI) or γAI-CTF-1 by immunoblot analysis with anti-Cγ Ab (Fig. 8A). Notably, infected cells coexpressing myc-Pcdhα4/myc-PcdhγAI exhibited weak accumulation of the immunoreactive band corresponding to the full-length myc-PcdhγAI (~125%) (Fig. 8B), compared to cells expressing myc-PcdhγAI/GFP. Furthermore, the weak accumulation of full-length myc-PcdhγAI was accompanied by a threefold reduction of the γAI-CTF-1 in neurons coexpressing myc-Pcdhα4/myc-PcdhγAI (~29%) (Fig. 8B), compared to myc-PcdhγAI/GFP-coexpressing cultures. These data support the notion that the expression of Pcdhα4 could render PcdhγAI more resistant to surface processing, presumably by the formation of α/γ-Pcdh heteromers. The decrease in myc-PcdhγAI turnover could reflect reduced MMP-mediated ectodomain shedding or attenuated γ-secretase cleavage of PcdhγAI in neurons. We thus repeated the experiments on γ-Pcdh cleavage in the presence of DAPT and found the same weak accumulation of the full-length myc-PcdhγAI and threefold reduction of the corresponding γAI-CTF-1 as in absence of DAPT, indicating an altered susceptibility of PcdhγAI to MMP cleavage (data not shown). Since the overexpression of myc-PcdhγAI/GFP or myc-Pcdhα4/myc-PcdhγAI might lead to saturation of MMPs or the γ-secretase complex, we monitored the PS-IP of endogenous N-cadherin in DAPT-treated high-density cortical cultures expressing either myc-PcdhγAI/GFP (Fig. 8C, lane 1) or myc-Pcdhα4/myc-PcdhγAI (lane 2). DAPT treatment of the cultures was necessary for visualization of N-Cad/CTF-1 (Fig. 8C, lane 3). The expression of either myc-Pcdhα4/myc-PcdhγAI or myc-PcdhγAI/GFP had no significant effect on the processing of N-cadherin (Fig. 8D). This result indicates normal functioning of the MMP and γ-secretase complex in neurons overexpressing myc-Pcdhα4/myc-PcdhγAI or myc-PcdhγAI/GFP. Thus, the altered susceptibility to processing of PcdhγAI by coexpression of Pcdhα4 appears to reflect heteromer formation.

The impact of γ-Pcdh expression on α-Pcdh processing was less prominent. Immunoblot analysis of cultures infected with rAAV expressing myc-PcdhγAI/myc-Pcdhα4 and treated with DMSO or DAPT revealed a twofold increase in the immunoreactive band corresponding to the full-length protein (data

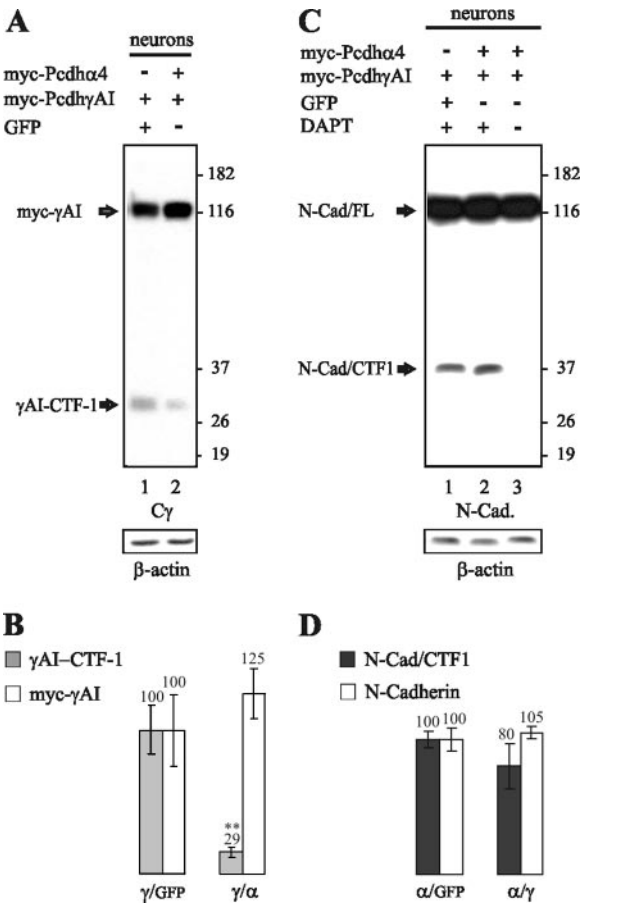

FIG. 8. Effects of myc-Pcdhα4 on myc-PcdhγAI cleavage in neurons. (A) Upper panel, immunoblot analysis with anti-Cγ Ab (Cγ) of protein lysates of DIV 14 rat cortical cultures double-infected with rAAVs expressing either myc-PcdhγAI/GFP (lane 1) or myc-PcdhγAI/myc-Pcdhα4 (lane 2) (molecular mass markers [in kilodaltons] are shown on the right). Lower panel, immunoblot of corresponding lysates with anti-β-actin Ab (β-actin) serving as the loading control. Above the immunoblots is a scheme representing the expression of myc-Pcdhα4, myc-PcdhγAI, or GFP in neurons. (B) Quantification of results shown in panel A. The bar graph includes the average values ± SEM, and significant differences (**, $P \leq 0.01$ by t test) for γAI-CTF-1 and myc-γAI in myc-PcdhγAI/GFP or myc-PcdhγAI/myc-Pcdhα4-expressing, double-infected, primary cortical cultures (as percentages of the amount in myc-PcdhγAI/GFP-expressing neurons; $n = 5$) are indicated. (C) Upper panel, immunoblot with anti-N-cadherin Ab (N-Cad.) of protein lysates of DIV 14 rat cortical cultures double-infected with rAAVs expressing either myc-PcdhγAI/GFP (lane 1) or myc-PcdhγAI/myc-Pcdhα4 (lanes 2 and 3). To better visualize the N-cadherin CTF-1 (N-Cad/CTF-1), cultures were treated with DAPT (lanes 1 and 2) or, as the control, with DMSO (lane 3). Lower panel, immunoblot of corresponding lysates with anti-β-actin Ab (β-actin) serving as the loading control. Above the immunoblot is a scheme representing the expression of myc-Pcdhα4, myc-PcdhγAI, GFP, and DAPT treatment in neurons. (D) Quantification of results shown in panel C. The bar graph includes the average values ± SEM, and significant differences (**, $P \leq 0.01$ by t test) for the C-terminal N-cadherin cleavage product (N-Cad/CTF-1) and full-length N-cadherin (N-Cad/FL) in myc-PcdhγAI/GFP- or myc-PcdhγAI/myc-Pcdhα4-expressing, double infected, primary cortical cultures treated with DAPT (as percentages of the amount in myc-Pcdhα4/GFP-expressing neurons; $n = 5$) are indicated.

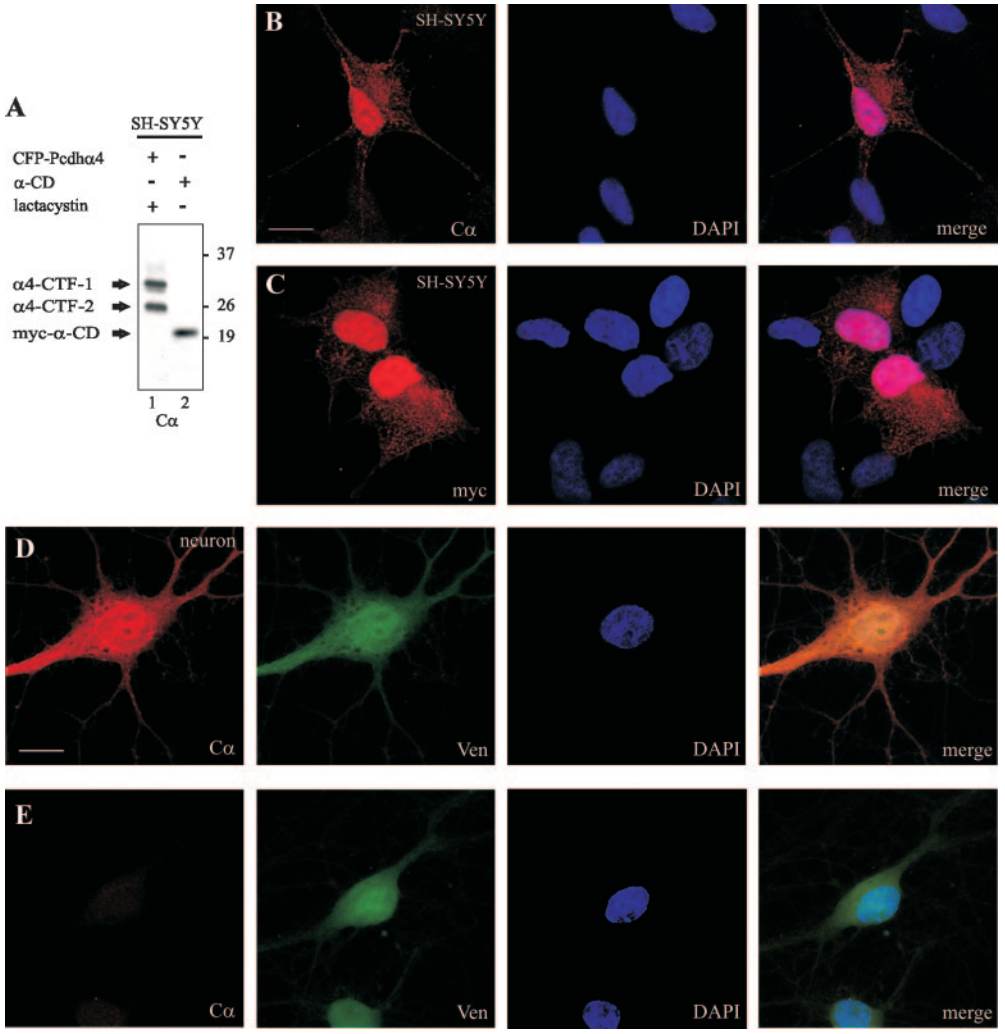

FIG. 9. Nuclear and cytoplasmic localization of the α-CD. (A) Immunoblot analysis with anti-Cα Ab (Cα) of whole-cell protein lysates of SH-SY5Y cells transiently expressing CFP-Pcdhα4 and treated with lactacystin (lane 1) or expressing myc-α-CD and treated with DMSO (lane 2). Above the immunoblot is a scheme representing the expression of CFP-Pcdhα4, α-CD, and lactacystin treatment of SH-SY5Y cells. (B) Immunocytochemistry with anti-Cα Ab (Cα; red) and DAPI (blue) of SH-SY5Y cells transiently expressing myc-α-CD. Colocalization of DAPI and Cα fluorescence is shown in pink (merge). (C) Immunocytochemistry with anti-myc Ab (myc; red) and DAPI (blue) of SH-SY5Y cells transiently expressing myc-α-CD. Colocalization of DAPI and myc fluorescence is shown in pink (merge). (D) Immunocytochemistry of DIV 21 rat primary hippocampal cultures infected with rAAV expressing myc-α-CD together with Venus (myc-α-CD internal ribosome entry site Venus; Ven). Anti-Cα immunoreactivity is shown in red, direct Venus fluorescence in green, and DAPI staining in blue. The overlay of the three images is shown in the rightmost picture (merge). (E) Immunocytochemistry of DIV 21 rat primary hippocampal cultures infected with rAAV expressing Venus. Anti-Cα immunoreactivity is shown in red (absence of the red signal demonstrates the specificity of the Cα Ab), direct Venus fluorescence in green, and DAPI staining in blue. The overlay of the three images is shown in the rightmost picture (merge). Scale bars = 10 μm.

not shown), compared to GFP/myc-Pcdhα4-expressing neuronal cultures. Unfortunately, we could not quantify α4-Pcdh CTF-1 abundance due to the high background produced by our anti-Cα Ab in neuronal lysates (see Fig. 5D).

In summary, these experiments provide evidence for the regulation of γ-Pcdh MMP cleavage via α-Pcdhs, whereas the effect of γ-Pcdh expression on α-Pcdh cleavage seems to be minor.

Nuclear translocation of the α-CD. The cytoplasmic domains of prominent targets of the γ-secretase complex, e.g., Notch, APP, N-cadherin, ErbB-4, SREBP-1, and γ-Pcdhs, can assume signaling functions in the cytoplasm and/or nucleus (1, 20, 21, 27, 34, 46). We investigated the putative nuclear translocation of α-Pcdh C-terminal domains by tracing the subcellular distribution of a C-terminal protein fragment containing the α-CTF-2 nuclear localization sequence. To this end, we constructed a vector for expressing the sequence encompassing the three constant exons of α-Pcdhs, fused N terminally to a myc epitope (myc-α-CD) (Table 1 and Fig. 9A). A homologous construct comprising only the conserved γ-Pcdh intracellular sequence was shown to have nuclear localization and activity. Confocal imaging of transiently transfected SH-SY5Y cells stained with anti-Cα Ab (Fig. 9B) and anti-myc Ab (Fig. 9C) revealed strong accumulation of the myc-α-CD in the nucleus compared to untransfected, adjacent cells, reminiscent of the almost exclusive nuclear localization of the γ-CD in heterolo-

gous cells (11). To investigate if myc-α-CD also locates to the nucleus in neurons, we infected rat hippocampal primary neurons with rAAVs expressing myc-α-CD/Venus or only Venus (Fig. 9D and E). The staining revealed cytoplasmic as well as nuclear localization of the myc-α-CD. In summary, these results may suggest a possible role of α-Pcdh C-terminal domain sequence in cellular and nuclear signaling.

DISCUSSION

Synapse formation is governed by pre- and postsynaptic transmembrane cell adhesion molecules of the immunoglobulin and cadherin superfamilies. Whereas some of these cell adhesion molecules may determine pre- and postsynaptic differentiation, others may contribute to the specificity with which synaptic connections form (reviewed in references 33, 40, 45, and 51). α- and γ-Pcdhs fulfill prerequisites for molecules mediating the formation of specific, functional neuronal circuits, as they are expressed differentially within single cells (17, 41, 43), mediate cell-cell adhesion (25, 28), form hetero- and homomers, and localize in part to synaptic membranes (24). Furthermore, they may adopt an intracellular signaling function, as recently suggested for γ-Pcdhs, which are subject to sequential MMP and γ-secretase proteolysis, generating a shedded variable fragment and a cytoplasmic γ-CTF-2 (9, 11, 30). In order to study the effect of α/γ-Pcdh homo- and heteromerization on the regulation of γ-Pcdh and α-Pcdh intramembrane processing, we sought to study the cleavage of α-Pcdhs in the neuronal plasma membrane. As an example for the 14 murine α-Pcdhs, we demonstrate PS-IP of Pcdhα4 at the neuronal cell surface by successive cleavage events mediated by an MMP and the γ-secretase complex, resulting in the release of α4-CTF-2. The committing step in PS-IP is the cleavage of the substrate by an MMP. For Pcdhα4, one of these MMPs is ADAM10, a member of the ADAM family of metallo-proteases, also responsible for the cleavage of N- and E-cadherins and PcdhγC3 (22, 30, 31). In contrast to N- and E-cadherin shedding, which can be induced by *N*-methyl-D-aspartate receptor activity, the regulation of γ-Pcdh ectodomain shedding in neurons is governed by AMPA receptors (21, 22, 30, 31). The close relationship of α- and γ-Pcdhs might predict AMPA receptor-regulated α-Pcdh shedding.

A second means of α-Pcdh cleavage regulation could be γ-Pcdh-dependent surface expression of α-Pcdhs, as shown in heterologous cell systems (e.g., SH-SY5Y and HEK293) (24). This raises the question of whether the neonatal death of γ-*Pcdh*$^{-/-}$ mice could result in part from a compound loss of α/γ-Pcdh surface delivery and the concomitant loss of signaling to the nucleus. Unexpectedly, based on the γ-Pcdh-dependent α-Pcdh surface delivery in heterologous cells, we failed to detect significant differences in α-Pcdh surface delivery between γ-*Pcdh*$^{+/+}$, γ-*Pcdh*$^{+/-}$, and γ-*Pcdh*$^{-/-}$ neurons, whether in primary neuronal culture or in vivo. We surmise that the surface delivery of α-Pcdhs, unaffected in γ-*Pcdh*$^{+/+}$, γ-*Pcdh*$^{+/-}$, and γ-*Pcdh*$^{-/-}$ neurons, may result from differential gene expression between heterologous SH-SY5Y cells and neurons, possibly by neuronal β-Pcdh expression. Hence, it will be interesting to determine if α-Pcdhs and β-Pcdhs can form heteromers and, consequently, if α-Pcdh surface delivery is affected in β-*Pcdh*$^{-/-}$ knockout mice.

A third way α- and γ-Pcdh cleavage is regulated could be by the formation of α- and γ-Pcdh heteromers in synapses. Here, we show that the virally mediated coexpression of Pcdhα4 strongly decreases the MMP-mediated ectodomain shedding of PcdhγAI in cultured neurons. Endogenous N-cadherin processing remained unaffected, excluding saturation of the MMP and γ-secretase complex by the overexpression of PcdhγAI and Pcdhα4. Thus, we predict that the formation of α-/γ-Pcdh heteromers might contribute to the modulation of Pcdh PS-IP. Indeed, given that individual neurons coexpress several isoforms of α- and γ-Pcdhs (3, 16, 17, 41, 43), the additional combinatorial possibilities afforded by α- and γ-Pcdh heteromer formation might aid in specifying neuronal connectivity and could result in altered levels of processed Pcdh complexes. This in turn should also affect intracellular signaling by α- and γ-CTF-2.

PS-IP of γ-Pcdhs results in the release of γ-CTF-2 in the cytoplasm and subsequent translocation into the nucleus (9, 11), where it may control transcriptional activation of target genes (11) by as-yet-unknown mechanisms. Since α-Pcdhs are proteolytically processed in a similar fashion and cytoplasmic α-Pcdh fragments can localize to the nucleus, such fragments might also play a role in transcriptional control of target genes. The α4-Pcdh CTF-2 has an estimated mass of ~26 kDa, most probably encompassing a small part of the variable cytoplasmic region and the entire constant region. γ-Secretase cleavage might occur within an intramembrane stretch of the variable α-Pcdh domain without a consensus motif, given that the presenilin cleavage sites among the known targets lack sequence conservation (47). Strikingly, the conservation of the α-Pcdh CD, comprising most of the α-CTF-2, suggests largely uniform signaling of the 14 α-Pcdh isoforms. It will be of interest to decipher the role of α- and γ-Pcdh CTF-2 signaling in cytoplasmic and nuclear compartments, which could be achieved by combining protein-protein interaction studies with gene expression profiling and chromatin IPr analysis.

ACKNOWLEDGMENTS

We thank Yair Pilpel for taking images, Pawel Licznerski and Tanjew Dittgen for help with the neuronal culture, Sabine Grünewald for help with the cell culture, Bart De Strooper for the presenilin 1/2 dko cell line, Rolf Sprengel and Pavel Osten for help with the rAAV system, and Boris Hambsch, Noam Pilpel, and Stefan Wilkening for helpful suggestions.

REFERENCES

1. **Brown, M. S., and J. L. Goldstein.** 1997. The SREBP pathway: regulation of cholesterol metabolism by proteolysis of a membrane-bound transcription factor. Cell **89:**331–340.
2. **Dittgen, T., A. Nimmerjahn, S. Komai, P. Licznerski, J. Waters, T. W. Margrie, F. Helmchen, W. Denk, M. Brecht, and P. Osten.** 2004. Lentivirus-based genetic manipulations of cortical neurons and their optical and electrophysiological monitoring in vivo. Proc. Natl. Acad. Sci. USA **101:**18206–18211.
3. **Esumi, S., N. Kakazu, Y. Taguchi, T. Hirayama, A. Sasaki, T. Hirabayashi, T. Koide, T. Kitsukawa, S. Hamada, and T. Yagi.** 2005. Monoallelic yet combinatorial expression of variable exons of the protocadherin-alpha gene cluster in single neurons. Nat. Genet. **37:**171–176.
4. **Fenteany, G., R. F. Standaert, W. S. Lane, S. Choi, E. J. Corey, and S. L. Schreiber.** 1995. Inhibition of proteasome activities and subunit-specific amino-terminal threonine modification by lactacystin. Science **268:**726–731.
5. **Fischer, O. M., S. Hart, A. Gschwind, N. Prenzel, and A. Ullrich.** 2004. Oxidative and osmotic stress signaling in tumor cells is mediated by ADAM proteases and heparin-binding epidermal growth factor. Mol. Cell. Biol. **24:**5172–5183.
6. **Fujiwara, T., K. Oda, S. Yokota, A. Takatsuki, and Y. Ikehara.** 1988. Brefel-

din A causes disassembly of the Golgi complex and accumulation of secretory proteins in the endoplasmic reticulum. J. Biol. Chem. **263:**18545–18552.
7. **Grimm, D., M. A. Kay, and J. A. Kleinschmidt.** 2003. Helper virus-free, optically controllable, and two-plasmid-based production of adeno-associated virus vectors of serotypes 1 to 6. Mol. Ther. **7:**839–850.
8. **Gschwind, A., S. Hart, O. M. Fischer, and A. Ullrich.** 2003. TACE cleavage of proamphiregulin regulates GPCR-induced proliferation and motility of cancer cells. EMBO J. **22:**2411–2421.
9. **Haas, I. G., M. Frank, N. Veron, and R. Kemler.** 2005. Presenilin-dependent processing and nuclear function of gamma-protocadherins. J. Biol. Chem. **280:**9313–9319.
10. **Hamada, S., and T. Yagi.** 2001. The cadherin-related neuronal receptor family: a novel diversified cadherin family at the synapse. Neurosci. Res. **41:**207–215.
11. **Hambsch, B., V. Grinevich, P. H. Seeburg, and M. K. Schwarz.** 2005. γ-Protocadherins, presenilin-mediated release of C-terminal fragment promotes locus expression. J. Biol. Chem. **280:**15888–15897.
12. **Hartmann, D., B. de Strooper, L. Serneels, K. Craessaerts, A. Herreman, W. Annaert, L. Umans, T. Lubke, A. Lena Illert, K. von Figura, and P. Saftig.** 2002. The disintegrin/metalloprotease ADAM 10 is essential for Notch signalling but not for alpha-secretase activity in fibroblasts. Hum. Mol. Genet. **11:**2615–2624.
13. **Herreman, A., D. Hartmann, W. Annaert, P. Saftig, K. Craessaerts, L. Serneels, L. Umans, V. Schrijvers, F. Checler, H. Vanderstichele, V. Baekelandt, R. Dressel, P. Cupers, D. Huylebroeck, A. Zwijsen, F. Van Leuven, and B. De Strooper.** 1999. Presenilin 2 deficiency causes a mild pulmonary phenotype and no changes in amyloid precursor protein processing but enhances the embryonic lethal phenotype of presenilin 1 deficiency. Proc. Natl. Acad. Sci. USA **96:**11872–11877.
14. **Herreman, A., G. Van Gassen, M. Bentahir, O. Nyabi, K. Craessaerts, U. Mueller, W. Annaert, and B. De Strooper.** 2003. γ-Secretase activity requires the presenilin-dependent trafficking of nicastrin through the Golgi apparatus but not its complex glycosylation. J. Cell Sci. **116:**1127–1136.
15. **Junghans, D., I. G. Haas, and R. Kemler.** 2005. Mammalian cadherins and protocadherins: about cell death, synapses and processing. Curr. Opin. Cell Biol. **17:**446–452.
16. **Kaneko, R., H. Kato, Y. Kawamura, S. Esumi, T. Hirayama, T. Hirabayashi, and T. Yagi.** 2006. Allelic gene regulation of *Pcdh*-α and *Pcdh*-γ clusters involving both monoallelic and biallelic expression in single Purkinje cells. J. Biol. Chem. **281:**30551–30560.
17. **Kohmura, N., K. Senzaki, S. Hamada, N. Kai, R. Yasuda, M. Watanabe, H. Ishii, M. Yasuda, M. Mishina, and T. Yagi.** 1998. Diversity revealed by a novel family of cadherins expressed in neurons at a synaptic complex. Neuron **20:**1137–1151.
18. **Lammich, S., E. Kojro, R. Postina, S. Gilbert, R. Pfeiffer, M. Jasionowski, C. Haass, and F. Fahrenholz.** 1999. Constitutive and regulated alpha-secretase cleavage of Alzheimer's amyloid precursor protein by a disintegrin metalloprotease. Proc. Natl. Acad. Sci. USA **96:**3922–3927.
19. **Lois, C., Y. Refaeli, X. F. Qin, and L. Van Parijs.** 2001. Retroviruses as tools to study the immune system. Curr. Opin. Immunol. **13:**496–504.
20. **Marambaud, P., J. Shioi, G. Serban, A. Georgakopoulos, S. Sarner, V. Nagy, L. Baki, P. Wen, S. Efthimiopoulos, Z. Shao, T. Wisniewski, and N. K. Robakis.** 2002. A presenilin-1/γ-secretase cleavage releases the E-cadherin intracellular domain and regulates disassembly of adherens junctions. EMBO J. **21:**1948–1956.
21. **Marambaud, P., P. H. Wen, A. Dutt, J. Shioi, A. Takashima, R. Siman, and N. K. Robakis.** 2003. A CBP binding transcriptional repressor produced by the PS1/epsilon-cleavage of N-cadherin is inhibited by PS1 FAD mutations. Cell **114:**635–645.
22. **Maretzky, T., K. Reiss, A. Ludwig, J. Buchholz, F. Scholz, E. Proksch, B. de Strooper, D. Hartmann, and P. Saftig.** 2005. ADAM10 mediates E-cadherin shedding and regulates epithelial cell-cell adhesion, migration, and beta-catenin translocation. Proc. Natl. Acad. Sci. USA **102:**9182–9187.
23. **Miyoshi, H., U. Blomer, M. Takahashi, F. H. Gage, and I. M. Verma.** 1998. Development of a self-inactivating lentivirus vector. J. Virol. **72:**8150–8157.
24. **Murata, Y., S. Hamada, H. Morishita, T. Mutoh, and T. Yagi.** 2004. Interaction with protocadherin-gamma regulates the cell surface expression of protocadherin-alpha. J. Biol. Chem. **279:**49508–49516.
25. **Mutoh, T., S. Hamada, K. Senzaki, Y. Murata, and T. Yagi.** 2004. Cadherin-related neuronal receptor 1 (CNR1) has cell adhesion activity with beta1 integrin mediated through the RGD site of CNR1. Exp. Cell Res. **294:**494–508.
26. **Naldini, L., U. Blomer, P. Gallay, D. Ory, R. Mulligan, F. H. Gage, I. M. Verma, and D. Trono.** 1996. In vivo gene delivery and stable transduction of nondividing cells by a lentiviral vector. Science **272:**263–267.
27. **Ni, C. Y., M. P. Murphy, T. E. Golde, and G. Carpenter.** 2001. γ-Secretase cleavage and nuclear localization of ErbB-4 receptor tyrosine kinase. Science **294:**2179–2181.
28. **Obata, S., H. Sago, N. Mori, M. Davidson, T. St. John, and S. T. Suzuki.** 1998. A common protocadherin tail: multiple protocadherins share the same sequence in their cytoplasmic domains and are expressed in different regions of brain. Cell Adhes. Commun. **6:**323–333.
29. **Phillips, G. R., H. Tanaka, M. Frank, A. Elste, L. Fidler, D. L. Benson, and D. R. Colman.** 2003. Gamma-protocadherins are targeted to subsets of synapses and intracellular organelles in neurons. J. Neurosci. **23:**5096–5104.
30. **Reiss, K., T. Maretzky, I. G. Haas, M. Schulte, A. Ludwig, M. Frank, and P. Saftig.** 2006. Regulated ADAM10-dependent ectodomain shedding of gamma-protocadherin C3 modulates cell-cell adhesion. J. Biol. Chem. **281:**21735–21744.
31. **Reiss, K., T. Maretzky, A. Ludwig, T. Tousseyn, B. de Strooper, D. Hartmann, and P. Saftig.** 2005. ADAM10 cleavage of N-cadherin and regulation of cell-cell adhesion and beta-catenin nuclear signalling. EMBO J. **24:**742–752.
32. **Sambrook, J., E. F. Fritsch, and T. Maniatis.** 1989. Molecular cloning: a laboratory manual, 2nd ed. Cold Spring Harbor Laboratory Press, Cold Spring Harbor, NY.
33. **Scheiffele, P.** 2003. Cell-cell signaling during synapse formation in the CNS. Annu. Rev. Neurosci. **26:**485–508.
34. **Schroeter, E. H., J. A. Kisslinger, and R. Kopan.** 1998. Notch-1 signalling requires ligand-induced proteolytic release of intracellular domain. Nature **393:**382–386.
35. **Serafini, T.** 1999. Finding a partner in a crowd: neuronal diversity and synaptogenesis. Cell **98:**133–136.
36. **Shapiro, L., and D. R. Colman.** 1999. The diversity of cadherins and implications for a synaptic adhesive code in the CNS. Neuron **23:**427–430.
37. **Shevtsova, Z., J. M. Malik, U. Michel, M. Bahr, and S. Kugler.** 2005. Promoters and serotypes: targeting of adeno-associated virus vectors for gene transfer in the rat central nervous system in vitro and in vivo. Exp. Physiol. **90:**53–59.
38. **Smalla, K. H., H. Matthies, K. Langnase, S. Shabir, T. M. Bockers, U. Wyneken, S. Staak, M. Krug, P. W. Beesley, and E. D. Gundelfinger.** 2000. The synaptic glycoprotein neuroplastin is involved in long-term potentiation at hippocampal CA1 synapses. Proc. Natl. Acad. Sci. USA **97:**4327–4332.
39. **Sugino, H., S. Hamada, R. Yasuda, A. Tuji, Y. Matsuda, M. Fujita, and T. Yagi.** 2000. Genomic organization of the family of CNR cadherin genes in mice and humans. Genomics **63:**75–87.
40. **Takai, Y., K. Irie, K. Shimizu, T. Sakisaka, and W. Ikeda.** 2003. Nectins and nectin-like molecules: roles in cell adhesion, migration, and polarization. Cancer Sci. **94:**655–667.
41. **Tasic, B., C. E. Nabholz, K. K. Baldwin, Y. Kim, E. H. Rueckert, S. A. Ribich, P. Cramer, Q. Wu, R. Axel, and T. Maniatis.** 2002. Promoter choice determines splice site selection in protocadherin alpha and gamma pre-mRNA splicing. Mol. Cell **10:**21–33.
42. **Tiscornia, G., O. Singer, M. Ikawa, and I. M. Verma.** 2003. A general method for gene knockdown in mice by using lentiviral vectors expressing small interfering RNA. Proc. Natl. Acad. Sci. USA **100:**1844–1848.
43. **Wang, X., H. Su, and A. Bradley.** 2002. Molecular mechanisms governing *Pcdh*-γ gene expression: evidence for a multiple promoter and *cis*-alternative splicing model. Genes Dev. **16:**1890–1905.
44. **Wang, X., J. A. Weiner, S. Levi, A. M. Craig, A. Bradley, and J. R. Sanes.** 2002. Gamma protocadherins are required for survival of spinal interneurons. Neuron **36:**843–854.
45. **Washbourne, P., A. Dityatev, P. Scheiffele, T. Biederer, J. A. Weiner, K. S. Christopherson, and A. El-Husseini.** 2004. Cell adhesion molecules in synapse formation. J. Neurosci. **24:**9244–9249.
46. **Weidemann, A., G. Konig, D. Bunke, P. Fischer, J. M. Salbaum, C. L. Masters, and K. Beyreuther.** 1989. Identification, biogenesis, and localization of precursors of Alzheimer's disease A4 amyloid protein. Cell **57:**115–126.
47. **Wolfe, M. S., and R. Kopan.** 2004. Intramembrane proteolysis: theme and variations. Science **305:**1119–1123.
48. **Wu, Q., and T. Maniatis.** 1999. A striking organization of a large family of human neural cadherin-like cell adhesion genes. Cell **97:**779–790.
49. **Wu, Q., T. Zhang, J. F. Cheng, Y. Kim, J. Grimwood, J. Schmutz, M. Dickson, J. P. Noonan, M. Q. Zhang, R. M. Myers, and T. Maniatis.** 2001. Comparative DNA sequence analysis of mouse and human protocadherin gene clusters. Genome Res. **11:**389–404.
50. **Yagi, T., and M. Takeichi.** 2000. Cadherin superfamily genes: functions, genomic organization, and neurologic diversity. Genes Dev. **14:**1169–1180.
51. **Yamagata, M., J. R. Sanes, and J. A. Weiner.** 2003. Synaptic adhesion molecules. Curr. Opin. Cell Biol. **15:**621–632.
52. **Zufferey, R., D. Nagy, R. J. Mandel, L. Naldini, and D. Trono.** 1997. Multiply attenuated lentiviral vector achieves efficient gene delivery in vivo. Nat. Biotechnol. **15:**871–875.